Cross-sectional transmission electron microscopic study of irradiation induced nano-crystallization of nickel in a W/Ni multilayer

2008 J. Phys.: Condens. Matter 20 235202

(http://iopscience.iop.org/0953-8984/20/23/235202)

J. Phys.: Condens. Matter **20** (2008) 235202 (6pp) doi:10.1088/0953-8984/20/23/235202

Cross-sectional transmission electron microscopic study of irradiation induced nano-crystallization of nickel in a W/Ni multilayer

Sharmistha Bagchi and N P Lalla

UGC-DAE Consortium for Scientific Research, University Campus, Khandwa road, Indore-452001, India

Received 20 November 2007, in final form 22 February 2008
Published 30 April 2008
Online at stacks.iop.org/JPhysCM/20/235202

Abstract

The present study reports the cross-sectional transmission electron microscopic investigations of swift heavy ion-irradiation induced nano-size recrystallization of Ni in a nearly immiscible W/Ni multilayer structure. Multilayer structures (MLS) of $[W(25\ Å)/Ni(25\ Å)]_{10BL}$ were grown on Si-(100) substrate by the ion-beam sputtering technique. The as-synthesized MLS were subjected to 120 MeV-Au^{9+} ion-irradiation to a fluence of $\sim 5 \times 10^{13}$ ions cm^{-2}. Wide-angle x-ray diffraction studies of pristine as well as irradiated W/Ni multilayers show deterioration of the superlattice structure, whereas x-ray reflectivity (XRR) measurement reveals a nearly unaffected microstructure after irradiation. Analysis of the XRR data using 'Parratt's formalism' does show a significant increase of W/Ni interface roughness. Cross-sectional transmission electron microscopy (TEM) studies carried out in diffraction and imaging modes (including bright-field and dark-field imaging), show that at high irradiation dose the intralayer microstructure of Ni becomes nano-crystalline (1–2 nm). During these irradiation induced changes of the intralayer microstructure, the interlayer definition of the W and Ni layers still remains intact. The observed nano-recrystallization of Ni has been attributed to competition between low miscibility of the W/Ni interface and the ion-beam induced mixing kinetics.

1. Introduction

Swift heavy ion-irradiation is a powerful tool used to induce controlled structural changes. Swift heavy ions (SHI) lose their energy in the target mainly via inelastic collisions leading to the excitation of the target electrons. The electronic energy loss (S_e) has been found to induce various modifications in the target material, which include creation of defects and intermixing, leading to alloy formation [1–7]. The atomic motion induced by SHI is associated with the transfer of the electronic energy, deposited by the ions, to the lattice of the target material. There are different propositions of electronic energy transfer in a target: (i) Coulomb spike model [8] and (ii) thermal spike model [9, 10]. According to the Coulomb spike model, a swift heavy ion while passing through an insulating material medium causes ionization of the medium around its path. However, this model loses its validity in the case of metals. The thermal spike model, on the other hand, assumes that the energy deposited initially in the electronic subsystem gets subsequently transferred to the atomic subsystem via electron–phonon coupling. Above a certain threshold S_{eth} of the electronic energy loss, the material within a few nanometers from the ion path melts for a duration of 10^{-12}–10^{-11} s. It is this transient molten state of the material during which atomic motion/displacement takes place. This molten material then may quench very fast to freeze in some disordered structure or recrystallize.

For heavy ions (like Au, Ag etc) very high rates of electronic energy deposition up to few tens of MeV nm^{-1} are reached. Such a huge amount of electronic excitation is known to induce on a nanometer scale damage creation, phase transformation, and amorphous track formation in a wide range of materials, including insulators as well as pure metals and metallic compounds. It is this aspect of the SHI, which is used for tailoring the material microstructure and its properties. A strong mixing effect as a result of electronic excitations has

been observed in miscible Ni/Ti bilayers [11] and Fe/Si [12] and immiscible Tb/Fe [13] multilayers.

Giant magneto resistance (GMR) multilayers comprising magnetic materials like Fe, Co or Ni with Ag, Au or Cu [12–16] have also been studied. Due to the mutual immiscibility of these metal combinations, the multilayer interfaces are chemically sharp and hence formation of magnetically dead layers at the interfaces is suppressed [14]. From GMR application point of view the combination of Mo, W with Ni, Fe would also be of some interest due to expected interface stability [15] of such combinations of refractory metals. GMR of 8% in Fe/Mo MLS at 4.2 K was reported by Yan *et al* [16]. The stability of interfaces of evaporated Fe/W MLS was studied by Majkova *et al* [17]. Certain attention is also paid to the very thin Co films on W monocrystals [18, 19]. Recently we have observed nearly immiscible stable superlattice MLS in W/Ni [15], which is promising for technological applications.

Most of the time the characterization of irradiation induced intermixing and alloying of layers in a multilayer is done by wide-angle x-ray diffraction (XRD), where a relatively broad peak may invariably lead to the wrong conclusion. The intermixing will be better characterized by a direct imaging method, such as transmission electron microscopy (TEM), which is also capable of producing diffraction evidence from localized areas. But to the best of our knowledge detailed TEM studies on such nearly immiscibility stable superlattice multilayer structures are sparse. Therefore in the present work we have carried out extensive transmission electron microscopy studies on the irradiated W/Ni multilayer ($\Delta H = -1$ kJ mol^{-1}) [20] under the influence of 120 MeV Au^{9+} ion-irradiation. The pristine and the irradiated multilayers were characterized through wide-angle x-ray diffraction (WAXD), x-ray reflectivity (XRR) and cross-sectional transmission electron microscopy (X-TEM).

2. Experimental details

W/Ni MLS of 10-bilayers with a bilayer structure of [W(25 Å)/Ni(25 Å)] were deposited on [100] silicon substrates employing an ion-beam sputtering technique. For ion-beam sputtering, a Kaufman type hot cathode Ar-ion source was used. The MLS grown on silicon will here after be termed as WNi-10BL-Si. The operating parameters of the ion source were 1 kV/25 mA. A base pressure of 1×10^{-7} Torr was achieved before deposition, and during deposition it was maintained at $\sim 4 \times 10^{-4}$ Torr. W and Ni targets were mounted on a rotary motion feed through to switch over from one to another. The multilayer-coated Si substrate was cut into (10 mm × 10 mm) size pieces and subjected to 120 MeV Au^{9+} ion irradiation up to 5×10^{13} ions cm^{-2} fluence on the 15UD Pelletron accelerator facility at IUAC, New Delhi.

As a necessary and preliminary characterization of the pristine and irradiated WNi-10BL-Si MLS, WAXD and XRR were carried out. XRR measurements were performed using a θ–2θ diffractometer configured to operate in symmetrical Bragg–Brentano geometry, and mounted on a rotating anode (Cu Kα). The specular reflectivity data were collected between

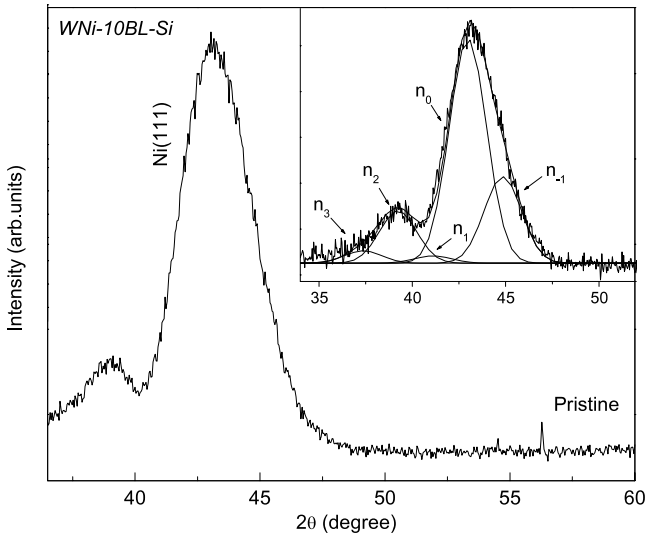

Figure 1. Wide-angle x-ray diffraction patterns of pristine WNi-10BL-Si multilayers. Inset shows the deconvolution of the unresolved satellite peaks, which are indexed as −1, 0, 1, 2, 3.

0° and 6° of 2θ in several parts, with a scan speed of 0.2° min^{-1} and in steps of 0.004°. The different parts of the data were later joined by proper normalization of the intensities.

WAXD measurements of the multilayer films were carried out using the same θ–2θ diffractometer without disturbing the sample alignment, done during XRR measurement. It was done simply by changing the divergence of the incident x-ray beam from 0.05° to 0.5°, and keeping the same alignment settings of the sample. This was done so as to ensure the best alignment of the multilayer surface with respect to the θ–2θ Bragg–Brentano geometry. Such an alignment is necessary for collecting proper intensity from an oriented MLS expected to give rise to superlattice reflections. The data were collected from (10° to 110°) 2θ so as to cover all intense Bragg reflections of W and Ni.

To have visual microstructural information, TEM studies were carried out, using a Tecnai-G^2-20 TEM facility operating at 200 kV. The cross-sectional specimens for TEM study were prepared following the standard technique [15]. Final thinning of the sample was done using Ar ion-beam polishing. Ion-beam polishing was done at 3 kV/20 μA and at a grazing incidence of 3° with respect to the sample surface.

3. Results

3.1. XRD and XRR studies

3.1.1. Pristine multilayers. The results of WAXD measurements carried out on a pristine sample of WNi-10BL-Si are shown in figure 1. The pristine sample shows an intense peak at 43.24° and a weak peak at 39.07°. At first glance these 2θ values appear to correspond to the most intense peaks of bulk Ni (111) and W (110), respectively. But these observed intense peaks are appearing only due to Ni(111). The most intense peak at 43.24° suggests [111] textured growth of the Ni layers. It should be noted that the full width at half maxima (FWHM) of the weak peak at 39.07° is nearly half of the

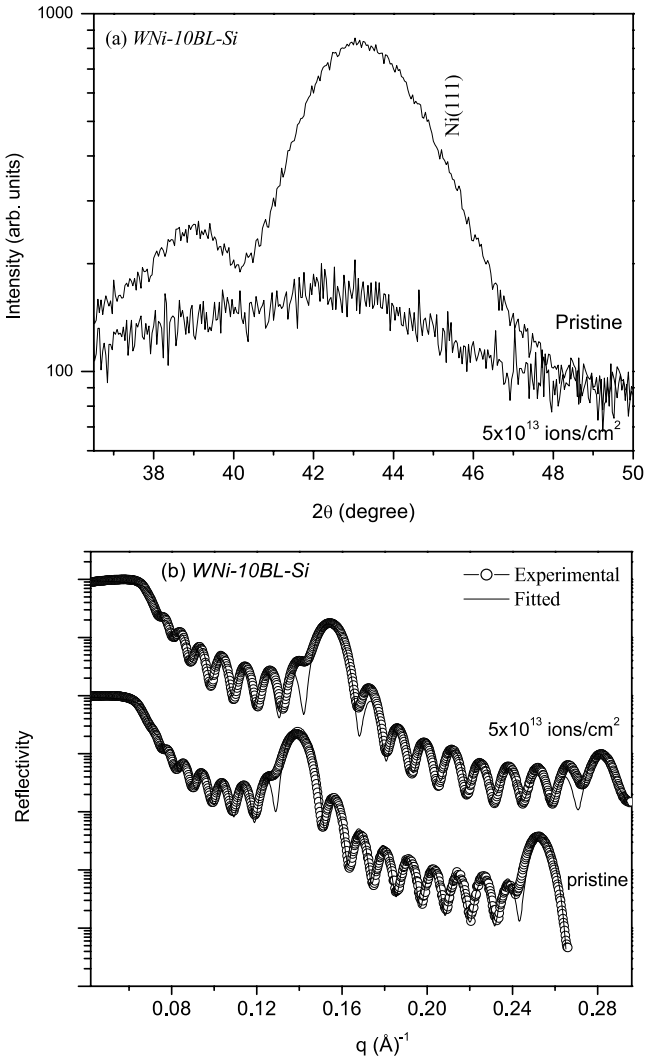

Figure 2. (a) Wide-angle x-ray diffraction patterns of pristine and irradiated WNi-10BL-Si multilayers. It can be seen that irradiation has destroyed the texture. (b) X-ray reflectivity patterns of the pristine and irradiated multilayer structure of WNi-10BL-Si. The XRR patterns are shifted for clarity.

FWHM of the intense peak at 43.24° and both the peaks are asymmetric. This indicates the presence of satellite peaks, which are quite close to the main peak. We could deconvolute and fit these merged satellite peaks, see inset of figure 1. These satellite peaks appear due to the formation of superlattice MLS. Further, the occurrence of ∼1.2° angular shift of the Ni(111) to lower 2θ side [15] suggests the supermodulus effect, giving rise to the superlattice formation. We could very well correlate the deconvoluted satellite peak positions with the bilayer period (Λ), which is given by the relation $1/d_{\text{ave}} \pm n/\Lambda$ around the main peak arising due to average interplanar spacing d_{ave} [15]. From the FWHM of the superlattice peaks we could estimate the structural correlation length of the superlattice MLS to be 49 ± 3 Å.

3.1.2. Irradiated multilayers. WAXD patterns recorded for pristine and irradiated WNi-10BL-Si MLS are shown in figure 2(a). It can be seen that the WAXD patterns

Table 1. Table showing the values of fit parameters, such as layer thickness and interface roughness of pristine and irradiated WNi-10BL-Si obtained using 'Parratt formalism'.

Irradiated dose WNi-10BL-Si	Layer thickness (Å) error of (±1 Å)		Interface roughness (Å) error of (±2 Å)	
	W	Ni	W	Ni
Pristine	25	26	4.5	2
5×10^{13} ions cm^{-2}	20	24	5.5	3.6

have changed quite drastically after ion-irradiation at 5×10^{13} ions cm^{-2}. The integrated peak intensity has decreased and FWHM increased. To estimate the integrated intensity and the FWHM, the profile of the major peak in the WAXD pattern was fitted with a pseudo-Voigt profile function. For WNi-10BL-Si the FWHM of the peak at 43.29° broadens by two-fold and its integrated intensity decreased by several orders of magnitude after irradiation. The superlattice peak almost disappears. These features definitely indicate that irradiation induced microstructural changes in the MLS are severe. The textured microstructure of the pristine MLS has completely transformed to either amorphous or nano-crystalline after ion-irradiation.

Figure 2(b) shows the XRR patterns corresponding to pristine as well as irradiated multilayer samples. The XRR patterns of the pristine multilayers clearly show well-defined Bragg peaks up to the second order. The irradiated MLS also shows Bragg peaks up to second order but the intensities have now slightly decreased and the peak positions are now shifted systematically towards the higher angle side. The decrease of the intensity and shift in the positions of the Bragg peaks indicates an increase of interface roughness and layer densification on ion-irradiation up to the fluence of 5×10^{13} ions cm^{-2} [21]. To extract the values of structural and interface parameters such as layer thickness and interface roughness, the XRR data were fitted using 'Parratt's formalism' [22]; the values of the fit parameters are listed in table 1. The obtained values of the layer thickness and interface roughness do show that the interface roughness has increased on irradiation from 4.5 to 5.5 for W and 2 to 3.6 for Ni. The increased interface roughness of the Ni layer is suggestive of nano-recrystallization of the Ni layer.

3.2. Cross-sectional TEM studies

For direct observation and better understanding of the irradiation induced microstructural changes, comparative X-TEM investigations on pristine as well as irradiated multilayers of WNi-10BL-Si were carried out employing imaging and selected area diffraction (SAD) modes on X-TEM samples. Figures 3(a)–(d) show the (a) X-TEM micrographs and (b) SAD patterns taken from the pristine WNi-10BL-Si multilayer sample. The inset of figure 3(a) shows typical EDAX spectra collected from X-TEM samples of a pristine WNi-10BL-Si multilayer. At every point in the sample we found nearly equal presence of W and Ni. This confirms that there is nearly 50–50% W and Ni in the MLS. The TEM micrograph in figure 3(a), shows nearly equal width black and

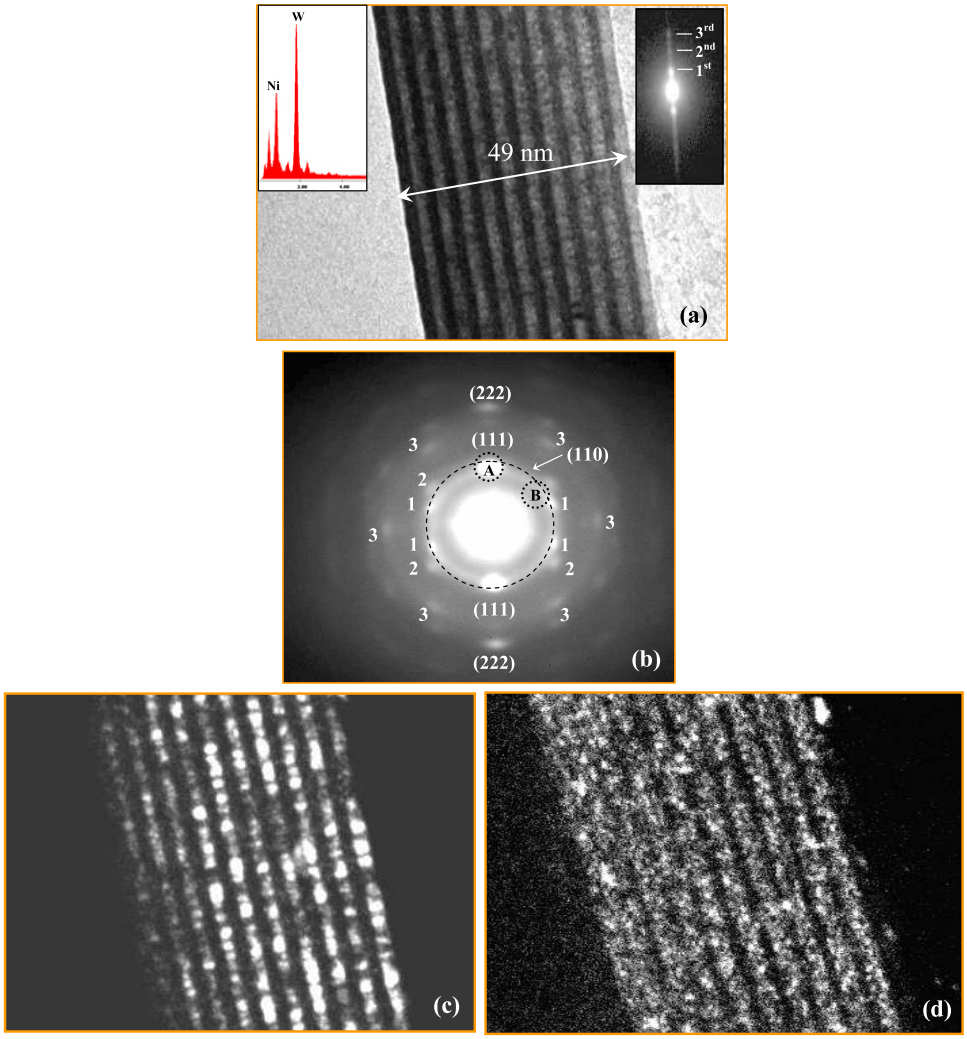

Figure 3. Cross-sectional TEM (a) micrograph of pristine WNi-10BL-Si multilayer. The equal width black and white strips correspond to W and textured Ni layers respectively. Corresponding wide-angle SAD patterns are shown in (b). The inset on the left side in (a) shows typical EDAX spectra from the samples. The one on the right side shows the low-angle SAD. In the SAD pattern (b) reflections of the same type have been given the same number. These numbers are 1-Ni(111), 2-Ni(200) and 3-Ni(220). The intense (111) and (222) reflections indicate the [111] textured growth of the film. The 4-weak 1-Ni(111) and 2-Ni(200) type reflections occurring symmetrically indicate random azimuthal orientation of the Ni layers about [111]. The axial dark-field images correspond to (c) (111) textured Ni and (d) nano-crystalline W layer.
(This figure is in colour only in the electronic version)

white strips of W and Ni [15], occurring periodically with a period of ∼50 Å. It clearly shows a well-defined growth of Ni and W layers. The inset shows the low-angle SAD from the multilayer structure. Bragg spots occurring up to the third order have been indicated. The wide-angle SAD pattern is shown in figure 3(b). The intense spots correspond to Ni(111) and (222). These indicate the [111] textured growth of Ni layers perpendicular to the film plane. The complete analysis of the diffraction pattern in figure 3(b) revealed that the [111] direction of each Ni grain is parallel and oriented perpendicular to the film plane. The symmetrical presence of {200}-type (marked-2) and other {111}-type (marked-1) reflections reveals an isotopic azimuthal orientation of the grains about [111]. The degenerate reflections have been marked by the same number, see caption of figure 3(b). The occurrence of a rather diffuse innermost ring corresponds to W(110). This shows that the W is in nano-crystalline form. Axial dark-field images were taken from the (111) spot of Ni (**A**) and a portion (**B**) of the diffuse ring due to W(110). These are shown in figures 3(c) and (d). Well-defined growth of Ni layers can be realized in figure 3(c). Each Ni layer is bright throughout the field of view, indicating that these layers are all textured. The fine line feature present in each Ni layer is due to the presence of [110] type stacking faults, typical of fcc structures. As is clear from the dark-field image in figure 3(d), W layers are also well formed. But the fine grain-like contrast indicates that the W layer is formed of nano-crystalline grains of ∼1 nm, and therefore we get quite a diffused (110) ring of W. The observed low structural coherence of ∼50 Å of the pristine superlattice multilayer structure is probably due to this nano-crystalline W. Figures 4(a)–(c) show the (a) X-TEM micrographs and (b) SAD patterns taken from the irradiated WNi-10BL-Si multilayer sample. The inset of figure 4(a) shows the X-TEM micrographs of the

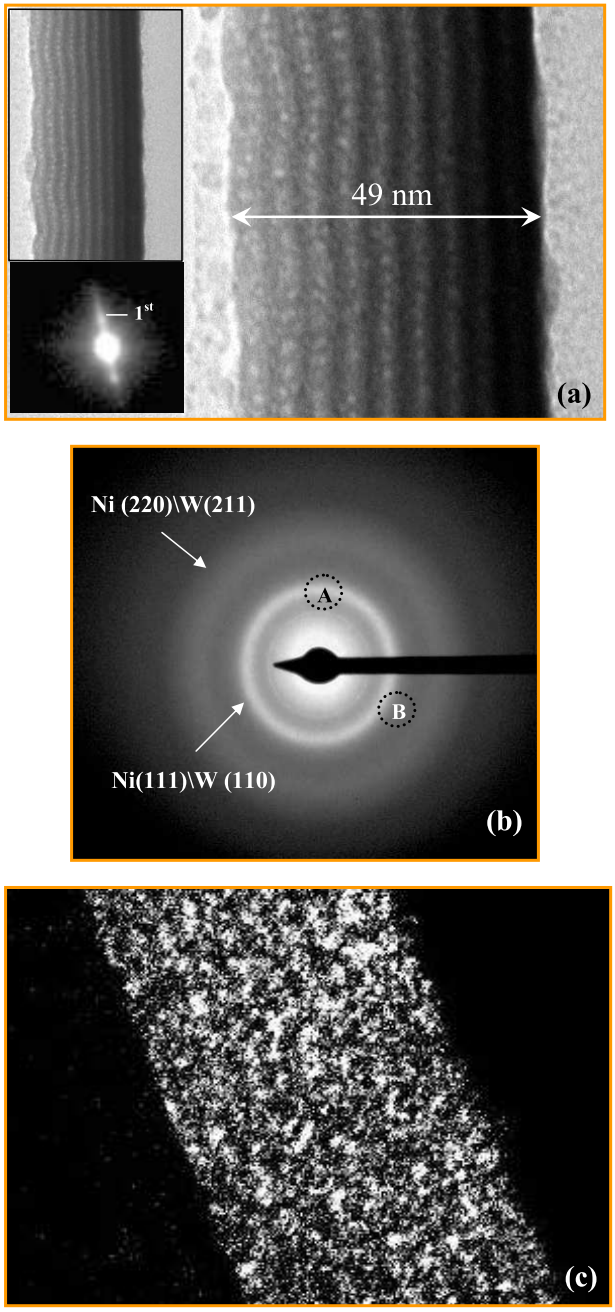

Figure 4. Cross-sectional TEM micrographs of (a) 5×10^{13} ions cm^{-2} irradiated WNi-10BL-Si multilayer. The micrograph in (a) shows irradiation induced nano-crystallization of each Ni layer without any intermixing of W and Ni. The continuous and broad diffraction rings of the SAD in (b) reveal the random aggregation of nano-crystalline Ni. (c) shows the axial dark-field image taken from region (B) of the ring. A layer contrast due to nano-crystalline Ni can be seen.

irradiated WNi-10BL-Si MLS. It can be vividly compared that the interlayer contrast is still intact, but the intralayer contrast has drastically changed. The intralayer contrast is a typical bright-field contrast expected from a nano-crystalline aggregate. This depicts that ion-irradiation has induced a textured to nano-crystalline transformation of the individuals layers. The observed alternate black and white layer contrast basically arises due to Z-contrast of W and Ni layers [15]. The appearance of Z-contrast even in the irradiated MLS depicts that although the swift heavy ion-irradiation has been able to change the intralayer microstructure of the Ni layer, from textured to nano-crystalline, individual W and Ni layers are chemically still unmixed. Irradiation induced textured to nano-crystalline transformation of the intralayer microstructure can also be clearly realized through the comparison of the SAD patterns shown in figures 3(b) and 4(b). The occurrence of continuous but rather broad diffraction rings clearly exhibits the aggregation of nano-crystalline Ni and W. The rings have been indexed with the intense reflections of Ni and W. The clear presence of (111) Ni and (220) Ni diffraction rings clearly depicts that the fcc structure of the Ni is still intact and no alloying has taken place. Since the intense central part (**A**) of the Ni(111) diffraction ring is also mixed with the broad diffraction rings due to W(110), it was impossible to image the nano-crystalline Ni layer in the dark-field. Therefore an axial dark-field was taken from the outer-region (**B**) of the (111) ring where the chance of W(110) contribution is negligible and the diffracted intensity would be mostly due to (111) and (200) of Ni. Figure 4(c) exhibits the axial dark-field taken from the region (**B**) of the ring. The layer contrast due to nano-crystalline Ni can be seen. This indicates that the Ni layer is chemically intact and no alloying has taken place, during ion-irradiation. The low-angle SAD pattern, as shown in the inset of figure 4(a), clearly shows the presence of the first Bragg spot. This indicates that the ion-beam has not been able to mix the layers. Another very interesting effect observed in the irradiated MLS is the puckeredness of the upper layers, which gradually vanishes towards the substrate. Keeping in view that the X-TEM specimens for pristine and irradiated samples were prepared following the same procedure; the observed puckeredness of the layer is purely due to the high dose of swift heavy ion-irradiation. It so appears that the ion-irradiation induced microstructural changes in the MLS cause a gradient of lateral expansion in the layers. Since the expansion has a gradient along the film thickness, the upper layers, which expand more, will get puckered to accommodate themselves in the same allowed substrate area.

4. Discussions

These contrasting results clearly depict the difference in interlayer and intralayer mixing effects of the 120 MeV Au^{9+} ions. This has been vividly approved by the cross-sectional TEM micrograph of the irradiated multilayer. During ion-irradiation the ions lose their energy through electronic (S_e) and nuclear (S_n) loss processes. Swift heavy ions, such as 120 MeV Au^{9+}, lose most of their energy through an electronic excitation loss process, nuclear loss is very small. Using TRIM [23] simulation we could calculate S_e for WNi-10BL-Si MLS to be 40.4 keV nm^{-1} for W and 36.7 keV nm^{-1} for Ni. The S_n was calculated to be 1.04 keV nm^{-1} for W and 0.7 keV nm^{-1} for Ni. Densities of W and Ni taken for these calculations are $\sim$18 g cm^{-3} and $\sim$7 g cm^{-3} respectively. A high electronic energy deposition (HEED) is known to cause atomic displacement, leading to annealing

of defects, creation of damage or even phase transformation in solids. Mobility induced under HEED has also caused crystallization [24] of amorphous silicon and alloying [24], in an Fe–Si system, which has large negative heat of mixing $\Delta H = -39$ kJ mol^{-1} [20]. For the W–Ni system the heat of mixing is only $\Delta H = -1$ kJ mol^{-1} [20]. Such a small negative heat of mixing has effectively been found to be immiscible [25]. Therefore in the present case also the miscibility will be much lower, and the chance of intermixing during ion-irradiation is quite low. It so appears that ions with such a high-energy deposition are acting as thermal spikes causing local melting, since W and Ni are nearly immiscible and the molten Ni recrystallizes to 1–2 nm size without any significant reaction with W. Due to the nearly immiscible nature of the W–Ni interface the corresponding chemical driving force is not strong enough to cause significant intermixing. The recrystallization of individual metal layers to nano-crystals will wash out the texturing of the layers.

5. Conclusion

Based on the above described analysis of the results of TEM studies on WNi-10BL-Si MLS subjected to swift heavy ion-irradiation, it can be concluded that the W–Ni system forms a superlattice multilayer structure consisting of Ni layers preferentially oriented along [111]. The swift heavy ion-irradiation affects the interlayer and intralayer features in different ways. On irradiation the textured growth of the multilayer deteriorates heavily due to recrystallization of the individual layers into randomly oriented nano-crystals. Whereas due to the nearly immiscible nature of the W–Ni system the interface of the multilayer structure remains less affected. TEM results confirm the nano-crystalline structure of the Ni layers in the heavily irradiated W/Ni multilayer. These changes in the microstructures cause expansion of the upper layers of the multilayer structure, producing puckeredness.

Acknowledgments

The authors would like to acknowledge Dr P Chaddah the Director, Professor A Gupta the Center-Director, of UGC-DAE-CSR Indore for their interest in this work. The authors sincerely thank F Singh for his help during irradiation of multilayer samples at IUAC New Delhi. The authors are also thankful to Satish Potdar for his help during deposition of the multilayer samples.

References

[1] Iwase A, Sasaki S, Iwata T and Nihira T 1987 *Phys. Rev. Lett.* **58** 2450
[2] Bauer Ph, Dufour C, Jaouen C, Marchal G, Pacaud J, Grilhe J and Jousset J C 1997 *J. Appl. Phys.* **81** 116
[3] Thibaudau F, Cousty J, Balanzat E and Bou S 1991 *Phys. Rev. Lett.* **67** 1582
[4] Rumbolz C, Bolse W, Kumar S, Chauhan R S, Kabiraj D and Avasthi D K 2006 *Nucl. Instrum. Methods* B **245** 145
[5] Bhattacharya D, Principi G, Gupta A and Avasthi D K 2006 *Nucl. Instrum. Methods* B **244** 198
[6] Kumar S, Chauhan R S, Singh R P, Kabiraj D, Sahoo P K, Rumbolz C, Srivastava S K, Bols W and Avasthi D K 2003 *Nucl. Instrum. Methods* B **212** 242
[7] Jaouen C, Michel A, Pacaud J, Dufour C and Bauer Ph 1999 *Nucl. Instrum. Methods* B **148** 176
[8] Fleisher R L 1965 *J. Appl. Phys.* **36** 3645
[9] Wang Z G, Dufour C, Paumier E and Toulemonde M 1994 *J. Phys.: Condens. Matter* **6** 6733
[10] Toulemonde M, Dufour C and Paumier E 1992 *Phys. Rev.* B **46** 14362
[11] Leguay R, Dunlop A, Dunstetter F, Lorenzelli N, Brasleau A, Bridou F, Corno J, Pardo B, Chevallier J, Colliex C, Me-nelle A and Rouviere J L 1995 *Nucl. Instrum. Methods* B **106** 28
[12] Dufour C, Jaouen C, Marchal G, Pacaud J, Grilhe J and Jousset J C 1997 *J. Appl. Phys.* **81** 116
[13] Teillet J, Richomme F, Fnidiki A and Toulemonde M 1997 *Phys. Rev.* B **55** 11560
[14] Lai W Y, Pan C Y, Wang Y Z, Yan M L, Li S X and Yu C T 1996 *J. Magn. Magn. Mater.* **155** 358
[15] Bagchi S and Lalla N P 2007 *Thin Solid Films* **515** 5227
[16] Yan M L, Sellmyer D J and Lai W Y 1991 *J. Phys.: Condens. Matter* **9** L145
[17] Majkova E, Luby S, Jergel M, Anopchenko A, Chushkin Y, Barucca G, Cristoforo A, Mengucci P, Anna E D, Luches A, Martino M and Hsin-Yi Lee 2002 *Mater. Sci. Eng.* C **19** 139
[18] Garreau G, Farle M, Beaurepaire E and Baberschke K 1997 *Phys. Rev.* B **55** 330
[19] Gutjahr-Loeser Th, Sander D and Kirschner J 2000 *J. Magn. Magn. Mater.* **220** L1
[20] de Boer F R, Boom R, Mattens W C M, Miedema A R and Niessen A K 1988 *Cohesion in Metals* (North-Holland: Amsterdam)
[21] Dhuri P, Gupta A, Chaudhari S M, Phase D M and Avasthi D K 1999 *Nucl. Instrum. Methods* B **156** 148
[22] Parratt L G 1954 *Phys. Rev.* **95** 359
[23] Ziegler J F, Ziegler M D and Biersack J P 1985 *Stopping and Range of Ions in Solids* (New York: Pergamon) http://www.srim.org/SRIM/SRIM2006.htm
[24] Bauer Ph, Dufour C, Jaouen C, Marchal G, Pacaud J, Grilhe J and Jousset J C 1997 *J. Appl. Phys.* **81** 116
[25] Majkova E, Luby S, Jergel M, Chushkin Y, Anna E D, Luches A, Martino M, Mengucci P, Majni G, Kuwasawa Y and Okayasu S 2003 *Appl. Surf. Sci.* **208** 394